17th World Conference on Earthquake Engineering, 17WCEE
Sendai, Japan - September 27th to October 2nd, 2021

EXPERIMENTAL AND ANALYTICAL STUDY OF T-SHAPED REINFORCED CONCRETE WALLS UNDER CYCLIC LOADS

F. Rojas[1], F. Muñoz[2], L.M. Massone[3], M. Ruiz[4]

[1] *Assistant Professor, University of Chile, fabianrojas@uchile.cl*
[2] *M.Sc., University of Chile, fernando.munoz@idiem.cl*
[3] *Associate Professor, University of Chile, lmassone@uchile.cl*
[4] *Structural Engineer, IE3, mruiz@ie3.cl*

Abstract

Reinforced Concrete (RC) wall systems are the preferred lateral resisting system for mid-height residential buildings (10 to 30 stories) in Chile. Typically, due to architectural constraints the Chilean design practice results in complex cross-sectional geometry (T or C) and discontinuities in the first story for these walls, such as openings and flag-wall types. During the Mw 8.8 earthquake in 2010 in Chile, several slender wall structures with or without discontinuities at the first floors were damaged, showing spalling of the concrete cover, crushing of concrete, buckling and fractures of bars at the boundary elements of the walls. Due to these damages observed in T-shaped RC walls with and without discontinuity and in order to quantify the effect that would have the new code requirements proposed after the earthquake according to confinement, the present work studies the experimental result of three T-shaped RC walls tested under pseudo static cyclic loads and the analytical models based in the experimental test. The three T-shaped RC walls are designed and built to scale in order to represent the characteristics (dimension ratios, reinforcement ratio, and percentage of length in confined boundaries) that are present in most Chilean's buildings. The differences introduced between the three walls (confinement in the boundary elements and the discontinuity at the base of one of them), allow studying the effect of these characteristics in the distribution of strains, in the ductility and in the capacity of the RC T-Shaped walls. The experimental results are processed from photogrammetry analysis and the information obtained from the traditional instrumentation by LVDT's and Strain Gauges. From the results, it is possible to observe the increase in ductility due to adequate confinement, but not a considerable increase in capacity in walls. On the other hand, the discontinuity generates a reduction in capacity and ductility, and a concentration of the plastic deformation at the level of the discontinuity, compared to the T-Shaped wall without discontinuity. Finally, the parameters generated as: the capacity of resistance, ductility and deformation profiles, in addition to the study of the evolution of the plastic hinge length and the collaborating width of the flange, were used to validate models based on a nonlinear quadrilateral layered shell element, comparing global and local results. From the experiments and numerical models, it is possible to observe the change in the length of the plastic hinge with the roof displacement and the effect of the discontinuity of the flag type on it, which tends to restrict the length of the plastic hinge at the height of the discontinuity. Additionally, the collaborating width of the flange turns out to be greater than 80% from the first yielding until it covers the entire length for upper drifts before the loss of capacity of the wall due to the crushing of the concrete in the web.

Keywords: Reinforced Concrete, T-Shaped walls, Discontinuity, Cyclic Loading, Analytical Models.

1. Introduction

The recent Mw 8.8-earthquake in 2010, revealed some problems in the design of reinforced concrete walls in different types of structures in Chile, and in particular in boundary elements of walls with sections like C, U or T. The failure modes observed, which had not been observed in previous earthquakes in Chile, were mainly due to a high level of flexo-compression and lack of confinement at the boundary elements. These caused the quick loss of concrete covering and the buckling of the longitudinal reinforcement (Massone & Rojas 2012). In addition, another characteristic of the majority affected walls were the discontinuities that these had at their base, responding mainly to architectural requirements, which caused an excessive stress concentration (Massone et al. 2017).

Furthermore, the importance of confinement in the global behavior and capacity in T-shaped wall has been studied previously by Thomsen and Wallace (1995), and different researchers (Brueggen et al. 2017) which have shown the relevance of experimental tests for the different criteria of construction and geometry in another countries. For example, experimental test of rectangular walls with discontinuities at their base were carried out in Chile prior to this study, where the concentration of strains in the area of the flag wall was observed (Manriquez et al. 2017). However, there is not experimental data for T-Wall with discontinuities at their base or for the Chilean characteristic of boundary elements pre and post 2010 earthquake.

In order to study the modes of failure observed during the 2010 earthquake, the effect of the discontinuities, and the effect of the new Chilean requirements for confinement of RC T-shaped walls, an experimental an analytical research is carried out. In the experimental research, three specimens are tested under a quasi-static cyclic protocol with displacement control, and after theses three specimens are model numerically using a nonlinear layered shell element with 6 degrees of freedom per node developed by Rojas et. al (2019). The T-shaped walls are constructed at a scale of about 1/3, with the geometry and reinforcement ratio corresponding to a residential building according to Chilean typical characteristics of construction before and after the 2010 Mw 8.8 earthquake. These tests were carried out in the Laboratory of Structures at the University of Chile. In the next section, the description of the T-shaped wall, the experimental setup, and the results of the experiment and numerical analysis are presented.

2. Description of test specimens

2.1 Geometry and Reinforcement

The dimensions and reinforcement ratio of the three specimens (ET1, ET2, and ET3) are based on a study of real T-shaped walls on building of around 18 stories and two basements (Silva, 2016), which constitute examples of representative buildings in Chile. Due to the limitations of space present in the Laboratory, it is decided to carry out to scale the three specimens, resulting in a height of 3.35[m], with 2.65 [m] corresponding to the wall itself, 0.4 [m] for the foundation height that allows to fix the base and 0.3 [m] for the beam height that allows the adequate transfer of the vertical and lateral load. All test walls have a uniform thickness of 0.12 [m].

Walls ET1 and ET2 have a web length of 120 [cm] and a flange length of 90 [cm]. However, Wall ET3, has a reduction of 20 [cm] in the edge of its web at the base level (see Table 1 and Figure 1). The aspect ratio between the height of the web and the length of the walls is 2.2, which defines a type of wall controlled mainly by flexural behavior. The longitudinal reinforcement ratio at the boundary element of the web is 2.5% (d_b= 12 mm), and for the edge of the flange and also at the intersection between the web and the flange 1.8% (d_b= 10 mm) is used. On the other hand, the horizontal and vertical reinforcement consists of a double mesh with bars d_b= 6 mm at every 150 [mm], which gives a reinforcement ratio of 0.32%. It is important to note that the reinforcement of ET3 is identical to ET2. In Figure 1, the discontinuity stands out in blue, the slabs in light blue and the load transfer beam in yellow.

It is important to emphasize, that the walls have the presence of 2 slabs, which confer additional rigidity to the walls, to be able to represent the existing slabs between floors. In addition, only walls ET2 and ET3 have confinement reinforcement with hoops of $d_b = 6$ [mm] at the boundary elements. A complete summary of the reinforcements is presented at Table 2 and also are shown in Figure 2.

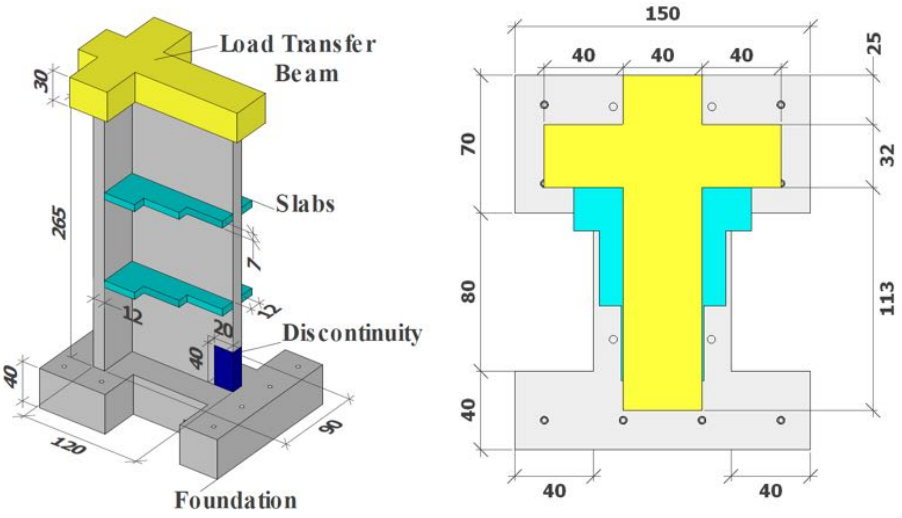

a) b)

Figure 1. Wall dimensions; a) 3D view; b) Plan View. (Unit: centimeters)

Table 1. Dimensions of Walls.

Parameter	ET1	ET2	ET3
Wall height [cm]	265	265	265
Web length l_w[cm]	120	120	100*
Flange length l_f[cm]	90	90	90
Thickness [cm]	12	12	12

* Due to 20[cm] discontinuity.

Table 2. Reinforcement of Walls.

Parameter	ET1	ET2	ET3
Web boundary reinforcement	4ϕ12	4ϕ12	4ϕ12
Flange boundary reinforcement	4ϕ10	4ϕ10	4ϕ10
Central reinforcement	16ϕ6	16ϕ6	14ϕ6
Confinement reinforcement	-	ϕ6	ϕ6
Transverse spacing (hoops, vertical and horizontal reinforcement) [cm]	150	150	150

2.2 Materials

To characterize the materials, tests were carried out to the concrete and the reinforcement bars. In the case of the concrete, compression tests were done at 7, 14, 28 days and the day of the test of the respective wall, as well as simple tensile tests to have the complete characterization of the concrete.

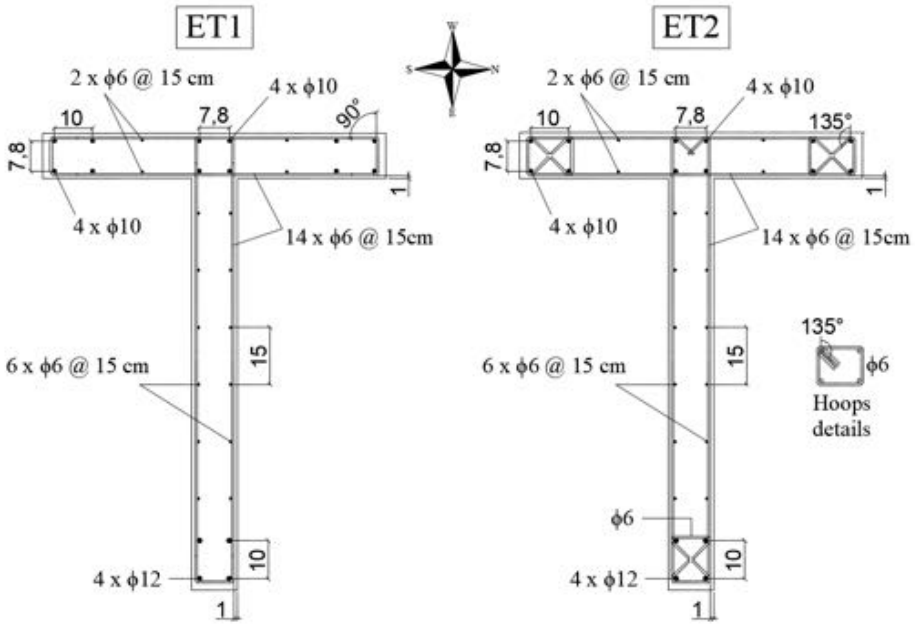

Figure 2. Details of reinforcement of ET1 and ET2. ET1 correspond to an unconfined configuration and the walls ET2 and ET3 correspond to the confined.

Tensile tests were also carried out for the rebar's of diameter (d_b), d_b = 6, 10 and 12 [mm] and also cyclic tests for the bars d_b = 12 [mm], with a buckling ratio L/d_b= 12.5, that represent ET1 and L/d_b= 6.25, that represent the separation between hoops and horizontal reinforcement presents at ET2 and ET3. Figure 3 shows some of the experimental results, as well as Tables 3 and 4.

Table 3. Concrete compression and tensile test.

Parameter	ET1	ET2	ET3
f_c' [MPa]	31.6	35.6	24.8
f'_t[MPa]	2.5	2.6	1.3
e_c [−]	0.027	0.026	0.020

f_c': Peak compression concrete strength at the day of experimental test.

f_t': Peak tensile concrete strength at the day of experimental test.

e_c: Strain at peak compressive stress.

Table 4. Tensile test for reinforcement.

Parameter	ϕ 6	ϕ 10	ϕ 12
f_y [MPa]	460	430	440
f_u [MPa]	855	738	768

f_y: Yield strength.

f_u: Ultimate tensile strength.

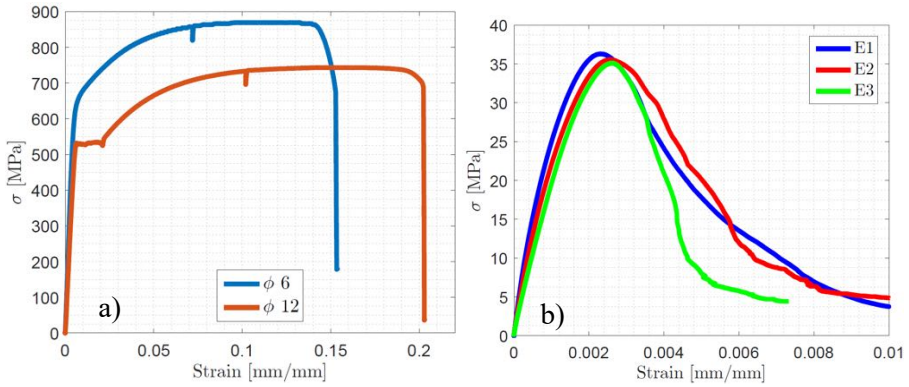

Figure 3. Examples of experimental results of materials. a) Tensile test for reinforcement bar ϕ6 and ϕ12. b) Concrete compression test of ET2 at the day of the wall test.

3. Experimental Setup

The experimental setup and the testing protocol for the three walls are identical. The test setup is presented in Figure 4, which highlights the slab and reaction wall, the wall under study, the hydraulic jacks that apply lateral and axial load and the system of frame that restrict displacement out of the load plane. The walls are tested under a quasi-static cyclic protocol with displacement control.

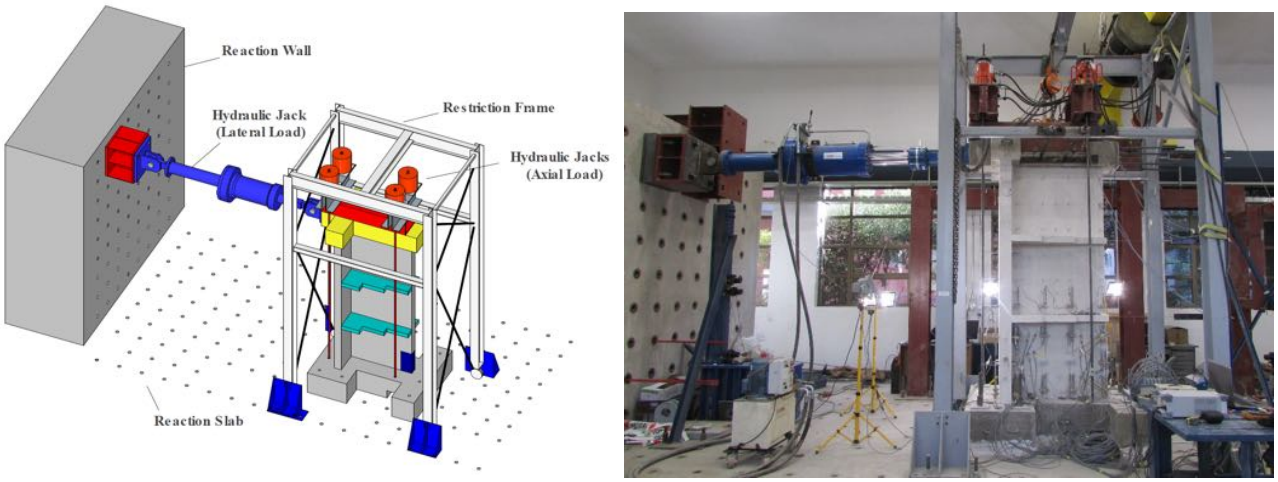

Figure 4. Experimental Setup for walls.

3.1 Instrumentation

All the walls tested were instrumented using LVDT's, Strain gages, Inclinometers and Load cells. In addition to this, the walls were monitored with 9 static cameras (0.08 pictures/seconds) to capture deformations and displacements using photogrammetry. The photographs allowed to detect in a more precise way the evolution of cracks and distribution of strain along the different faces of the wall.

For each test, an arrangement of 48 LVDT's was used (Figure 5), which were arranged to capture mainly the deformation in the first third of the wall, just under the first slab, where it is expected the concentration of the majority of the deformation, cracks and strains. In addition, two inclinometers are installed, one in the thickness of the web and one in the thickness of the flange (Figure 5), to be able to measure the angle with respect to the vertical of the first third of the wall outside the plane of the web, and the rotation of the flange.

In order to study the behavior of reinforcing bars, around 35 strain gages per wall were installed. The majority of these were located in the bars at the boundary elements, and in the horizontal and vertical

reinforcement, and hoops. Additionally, a strain gage was installed in a bar of the axial load system. Also, in ET3, two strain gages are installed to study also the overlap in the longitudinal bars in the area of the discontinuity.

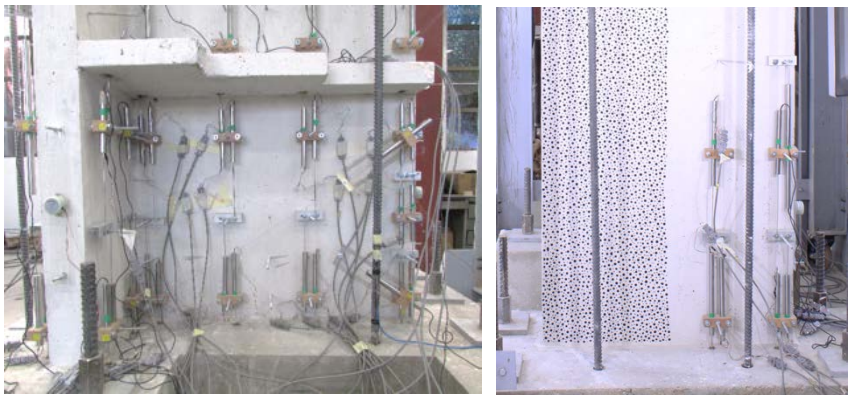

Figure 5. Instrumentation with LVDT's on wall ET2 (web on the left and flange on the right).

In addition, 9 digital cameras (Canon: series T3i, T5i and T6), were installed to photograph globally and locally the flange and the web (Figure 6). The latter to study the deformations and displacements with a digital image correlation process (DIC) with the NCorr software (Blaber et al. 2015). The data processing of LVDT's, Strain gages, Load Cells and Inclinometers, are generated from continuous readings in voltage during the length of the tests. As for the cameras, a data structure is generated that has the processed displacements and deformations every 12 seconds. The use of conventional instrumentation and photogrammetry allows to contrast the results between the two methodologies and also complement the results for the walls studies.

Figure 6. Experimental setup of digital cameras.

During each test, two load cells are used, one to control the axial load over the wall and another to measure the lateral load during the cycling protocol.

3.2 Loading Protocol

The test protocol consists of two parts. First, it is imposed the percentage of axial load that the walls should have and second, it is imposed the lateral load on the load transfer beam to reach the roof displacement target at each cycle. The axial load used is of around 0.085 $f_c' A_g$ (where f_c' is the peak compressive concrete strength and A_g is the gross wall cross-sectional area). The actual values used are presented in Table 5. It is

important to emphasize that the applied axial load correspond to an average load that is observed typically in Chilean buildings.

Table 5. Axial load ratio of walls

ET1	ET2	ET3
9.5%	8.5%	12%

The lateral displacement protocol, which is based on the propose by ACI374.1 (2005), consists in pseudo static cyclic displacements. The protocol includes two drifts in the elastic range with subsequent drifts until reaching the global failure in the compressed area of the web. The point of application of the load is at 2.8 [m] from the foundation and for each load drift there are 3 cycles. Figure 7 shows the protocol used.

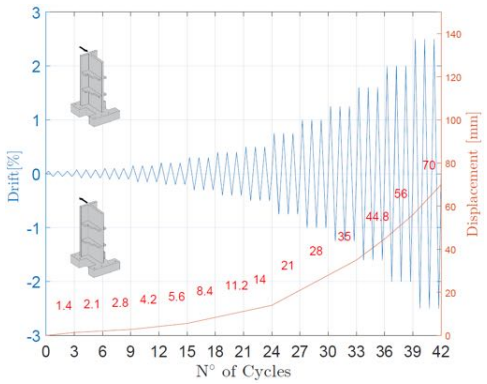

Figure 7. Experimental loading protocol.

4. Experimental Results

4.1 Results ET1

Figures 8a and 8b show the load-displacement curve for wall ET1 and final damage state, where a ductile behavior is observed for the direction when the flange is in compression, but not for the direction when the web is compressed. It can be clearly seen that once the ET1 wall reaches its maximum capacity, suddenly reduced its capacity, due to crushing of concrete and buckling of the bars.

The first cracks are observed at approximate drifts of 0.15 to 0.2%. For larger drifts, the cracks are mostly concentrated in the web, distributing mainly along two thirds of the wall. The spalling of concrete cover at the boundary element started in the last cycle of 1%. The strong drop observed at around 1.4% in the first cycle of 1.6% in the hysteresis corresponds to the spalling of all concrete cover exposing the entire reinforcement, which lead to the buckling of the longitudinal reinforcement. After this, fracture of rebar's is observed, ending all cycles of 1.6% with 4 bars ϕ12 fractured. This type of failure is the same of that observed in some Chilean buildings in 2010.

4.2 Results ET2

Figures 8c and 8d present the hysteretic behavior of the ET2 wall and final damage state. In terms of capacity, shares the same characteristics of the ET1 wall (as expected), but a remarkable increase in the ductility compared to the observed in ET1. The spalling of concrete cover is started in the first cycle of 1.25% up to the height of the first hoop. The strong effect of the confinement is observed from this point, because the bars did not show evident buckling until a large portion of the concrete core in the boundary element was crushed due to large drifts.

From the 1.6% drift, a gradual damage of the entire wall was observed; the concrete cover is completely lost, leaving the reinforcing bars exposed. The cracks expand to the second floor and it is possible to observe some cracks in the slabs. Finally, fracture of bars were generated at 2% drift, when the bars of the web were in tension, without significant damage to the flange, similar to the case of ET1.

4.3 Results ET3

The load-displacement curve of the wall ET3 is presented in Figure 8e. A similar behavior to wall ET2 is observed, in relation to the increase of the ductility. Despite the latter, it was observed a reduction in the capacity of the wall in the direction when the web was compressed, which could be attributed to the effect of the discontinuity, because the length of web is smaller than the other walls. The spalling of concrete cover started in the first cycle of 1%. The boundary bars rapidly buckle for drifts of 1.6 % and after that the wall lose its capacity and it is observed a great damage accumulated along the height of the discontinuity (Figure 8f).

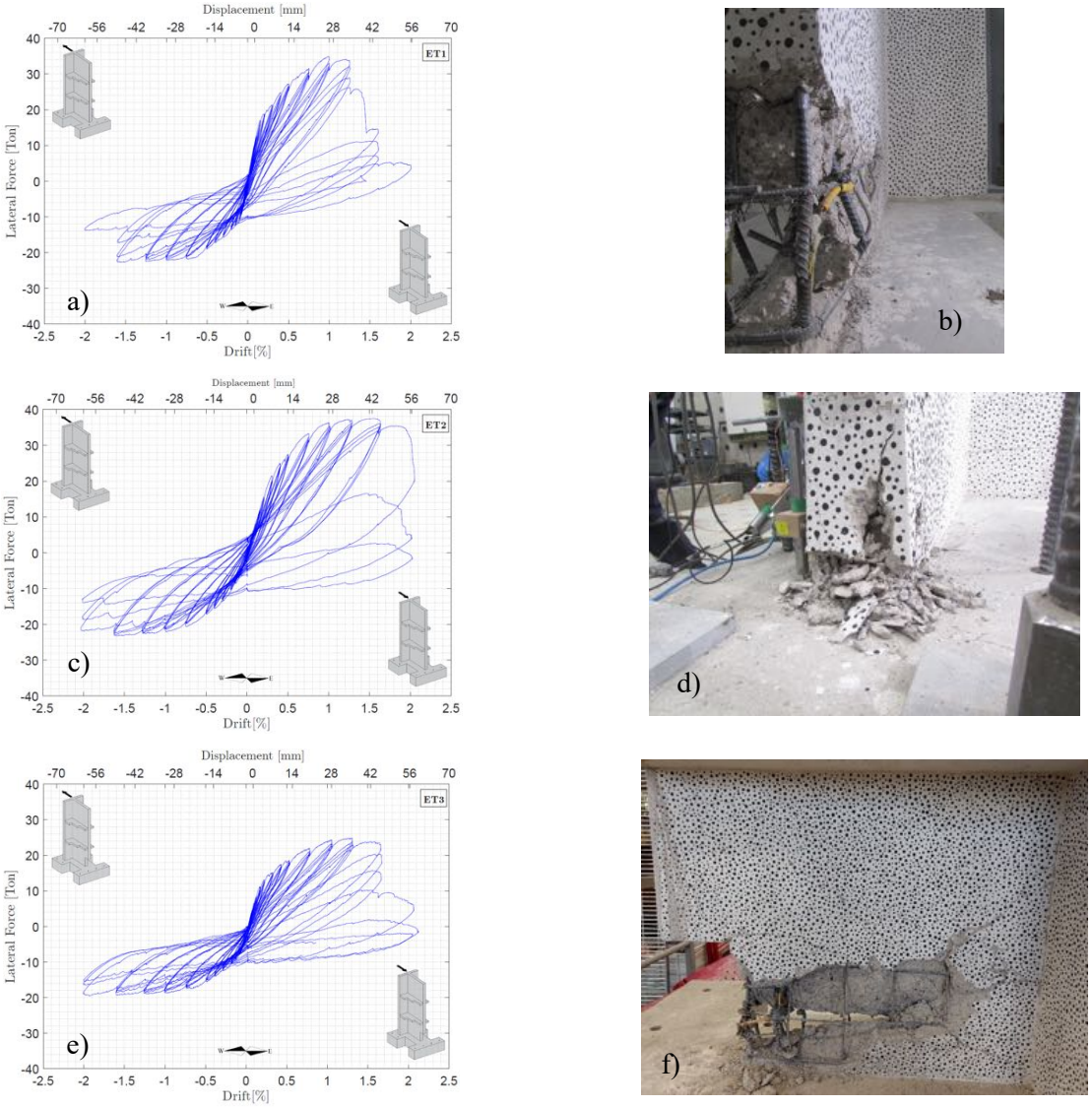

Figure 8. a) Load-displacement curve for ET1. b) Buckling of unrestrained reinforcement (end of test), c) Load-displacement curve for ET2. d) Spalling of concrete cover at 1.6 %. e) Load-displacement curve for ET3. f) Damage in the whole web.

4.4 Strain Measurements

Figure 9 present the strain distributions in the whole web in the first third of wall, which is obtained from photogrammetry, for the drift of 1% when the flange is in compression. These results indicates that the distribution of strains was concentrated in some cracks in height in wall ET1, whereas, the results of wall ET2 show a more uniform distribution in height, due to a good confinement at boundary elements.

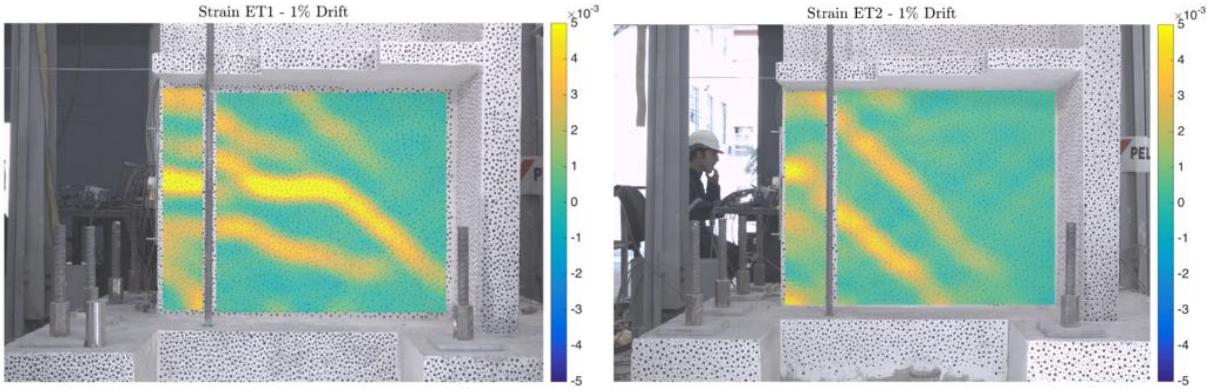

Figure 9. Strain distribution obtained from photogrammetry. a) ET1. b) ET2.

Figures 10a and 10b show strain profiles along the entire web at the first 50 [mm] from the base of the wall ET1 and strain profiles in height for the edge of the external side of the flange, all measured with LVDT. Figure 13 present ET1's results and Figures 10c and 10d ET2's. It's possible to observe higher compressions in wall ET1 than wall ET2 for the same level of drift. On the other hand, the behavior of flange is quite identical, except for the fact that the boundary elements in wall ET1 have a greater demand, before the spalling of concrete, when the web is in compression.

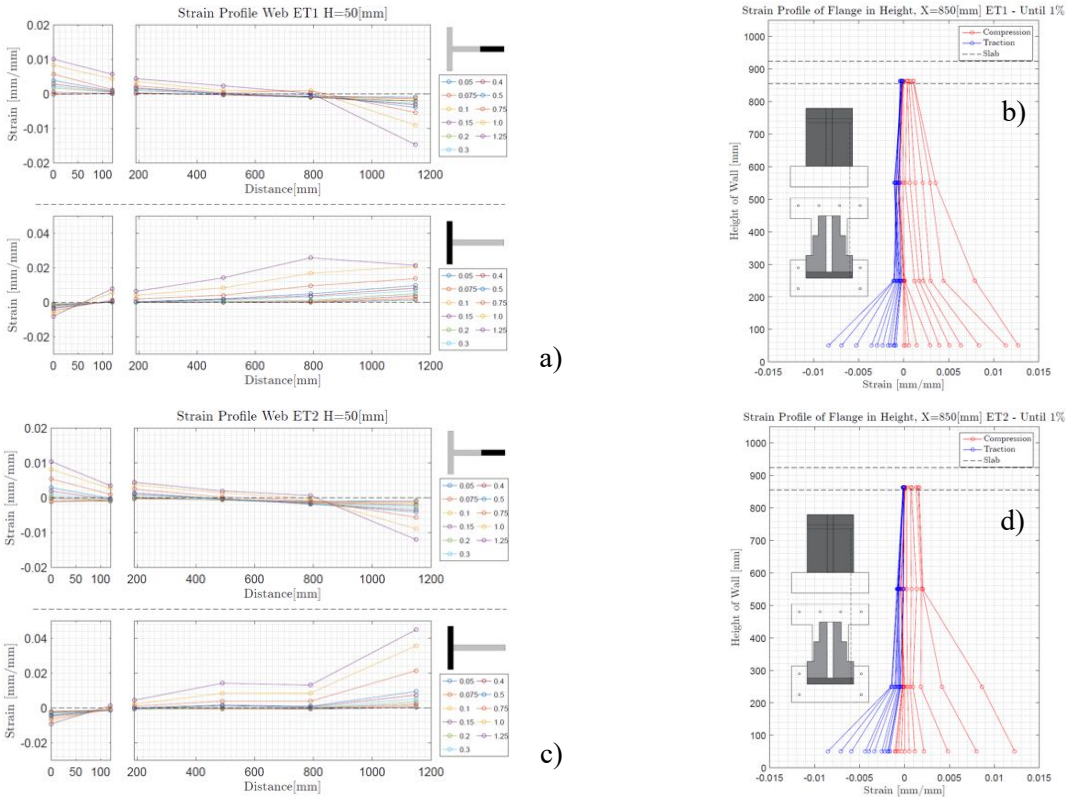

Figure 10. a) Strain profiles along the web (ET1). b) Strain profile of the flange at the boundary element (ET1), c) Strain profiles along the web (ET2). d) Strain profile of the flange at the boundary element (ET2).

5. Numerical analysis

5.1 No-Linear quadrilateral layered shell element for reinforced concrete

The numerical models in this section are generated using a no-linear layered quadrilateral shell element for reinforced concrete (Figure 11a) developed by Rojas et al. (2019). The element stiffness matrix and resisting force, assuming a fully bonded layered section and the element, has nine quadrature points with six degrees of freedom (DOF) per node, for a total of 24 DOF per element. For concrete, an orthotropic model formulation with rotating angle for the constitutive model for each concrete layer is used. In this formulation, it is assumed that the axes orthotropy coincide with the principal axes of deformation. For the uniaxial constitutive model of the concrete, the model proposed by Massone in 2006 with some modification to incorporate the cyclic behavior was used (Figure 11b). In the model, the compression envelope was defined with the curve defined by Thorenfeldt et al. in 1987, and later calibrated by Collins and Porasz in 1989 (Fig. 12a). The envelope of tension, implemented by Massone (2006), is the proposed by Belarbi and Hsu in 1994, which is divided into two sections, pre and post cracking. Moreover, for the steel mesh within the wall is modeled assuming that it is a homogeneous layer within the element, which requires considering an average stress-strain relationship to represent the action in the direction of the bar. For the uniaxial representation of the stress-strain curve of steel, the model of Menegotto and Pinto (1979) (Figure 11c) and the model of steel reinforcements with buckling proposed by Massone and Moroder (2009) are used.

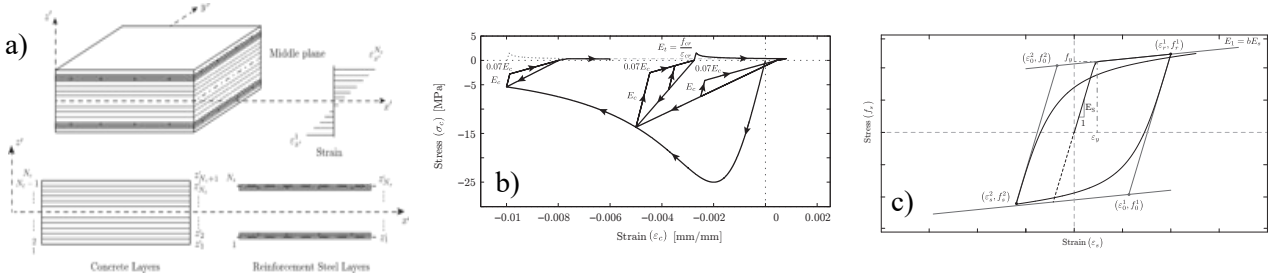

Figure 11. a) Shell transversal layered section, b) constitutive model for concrete and c) steel

In addition, the models (Figure 12) are developed considering: elastic elements in the foundation and in the load transfer beam and slabs, and inelastic elements in the rest of the wall, using the dimension and material properties defined in Tables 1 to 4. The foundation nodes are embedded in the base and lateral and axial load is applied along the nodes of the transfer beam in the direction of the web.

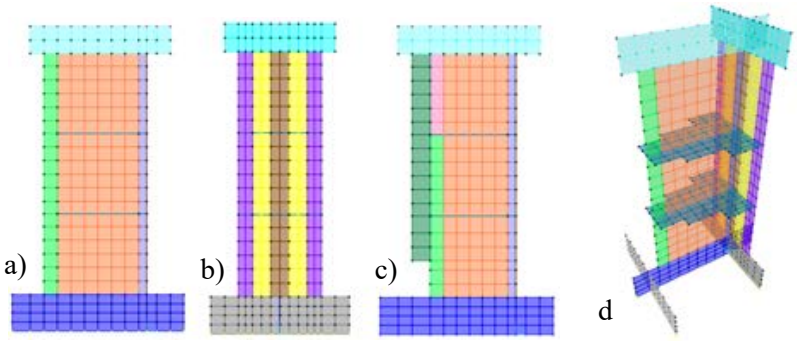

Figure 12. Finite element representation of wall ET1, ET2 and ET3: a) Web ET1 and ET2, b) Flange, c) Web ET3, and d) 3D Model ET1 and ET2

5.2 Results of the numerical models

In Figure 13, the comparison between the experimental and numerical load-displacement curves for the different walls are shown. It is observed that the model is able to reproduce the difference in confinement

between the ET1 and ET2 walls, which has a strong impact on the deformation capacity, but not on its strength capacity. On the other hand, it can be observed that the ET3 Wall has a ductile behavior like the ET2 Wall, but slightly lower, due to the presence of the discontinuity, which, as observed in the tests, concentrates the damage in this zone. The numerical models prove to be capable of replicating both the lateral force capacity of the wall and its deformation capacity with an error less than 10%. And in general, the only relevant difference in the comparison of results lies in the larger initial stiffness of the models, probably associated with unintended cracking of the specimens due to the construction, curing and test setup process.

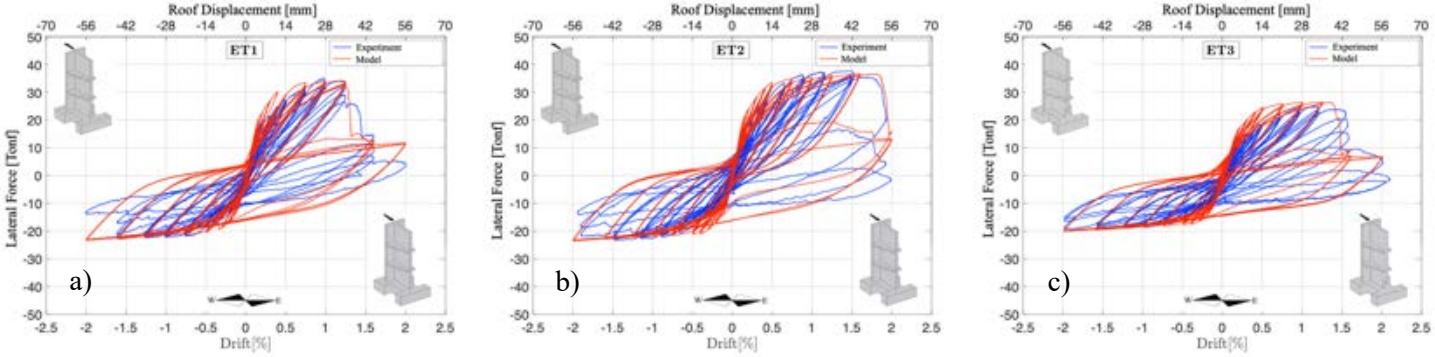

Figure 13. Experimental vs Numerical response for wall ET1 (a), ET2 (b) and ET3 (c)

Also, using the results of the LVDT and strain gages, located in the external part of the web, as well as the finite elements of the models located in the same area, an estimation of the effective width of the flange (stress weighting averages in the zone - $f_i w_i$, normalized by maximum stress - f_{fw}) can be obtained (Eq. 1). The normalized effective flange width for all walls is presented in Figure 14, which shows an excellent agreement between the numerical model and the experimental results.

$$b_{efec} = (\Sigma f_i w_i) / (\max (f_{fw})) \quad (1)$$

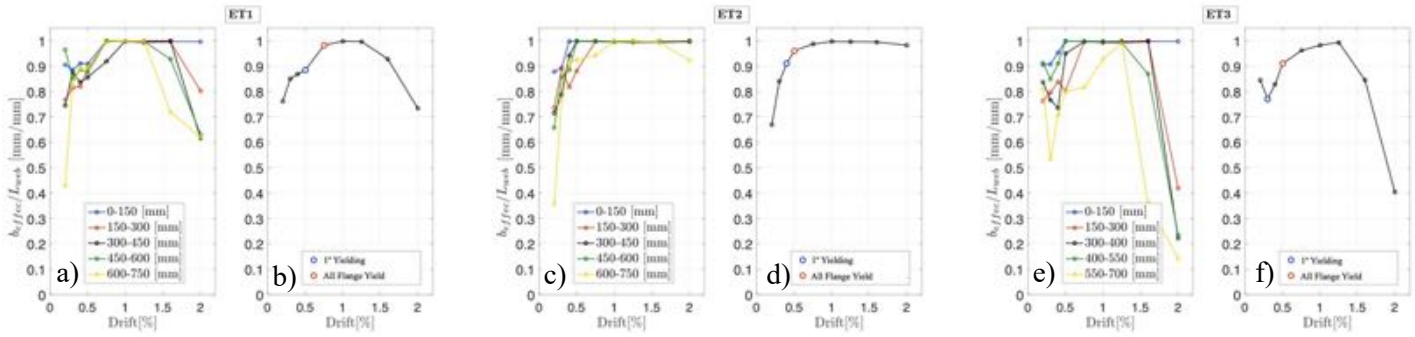

Figure 13. Effective flange width for wall ET1 (a: LVDTs b:Model), ET2 (c: LVDTs d:Model) and ET3 (e: LVDTs f:Model)

6. Conclusions

This work presents the results of a set of three T-shaped walls with different configurations of reinforcement and geometry tested under cyclic loading. From the results, it could be observed that the wall ET2, with a better confinement than ET1, presents an increase of about 50% of ductility, which confirms the type of failure in the boundary elements observed on several structures in the 2010 Chile earthquake due to the lack of confinement. On the other hand, the discontinuity in the wall ET3 generates a reduction in the capacity and ductility. It is also observed that the discontinuity generates a concentration of strains in the height of the discontinuity. In the case of the flange of walls, this had a similar behavior in the three tests, which did not suffer spalling of concrete cover or buckling of bars, showing a fairly ductile behavior.

In addition, the finite element models were able to reproduce correctly the capacity and maximum deformation of the ET1, ET2 and ET3 specimens, accurately describing the drift cycle where the failure occurs. Finally, in relation to the effective width calculated using the experimental results and the average stresses along the flange section from the numerical models, it can be observed that initially it is between 75% and 90% of the total length near the first yielding, and after grows quickly to the full length of the flange on higher drifts. This suggests that when designing the section in a T-shaped wall, the effective width would be equivalent to the entire section, independent of other parameters such as geometry or quantities, since once the walls reach yield, in one or more bars, the collaboration of the other bars is uniform, at least for the aspect ratios studied in this work.

6. Acknowledgments

This study was financially supported by Chile's National Commission on Scientific and Technological Research (CONICYT) for the project Fondecyt initiation into 2014 National Research Funding Competition under Grant No. 11140429, and National Research Funding Competition under Grant No. 1200709 from ANID (Agencia Nacional de Investigación y Desarrollo). The authors would also like to express their appreciation to all students, engineers and technicians of University of Chile who helped and gave supported in different stages of the complete study.

7. References

[1] ACI374.1 Acceptance Criteria for Moment Frames Based on Structural Testing and Commentary. American Concrete Institute. Reported by ACI Committee 374. 2005
[2] Belarbi H. y Hsu T., "Constitutive Laws of Concrete in Tension and Reinforcing Bars Stiffened By Concrete". ACI Structural Journal 91(4):465-474, 1994.
[3] Blaber, J., Adair, B., Antoniou, A. Ncorr: open-source 2D digital image correlation matlab software. Experimental Mechanics, 55(6): 1105-1122. 2015.
[4] Brueggen, B. L., French, C. E., Sritharan, S. T-Shaped RC Structural Walls Subjected to Multidirectional Loading: Test Results and Design Recommendations. Structural Engineering, 143(7), 04017040 :1-15. 2017.
[5] Collins MP, Porasz A. Bulletin D'Information no. 193: design aspects of high strength concrete. In: Shear strength for high strength concrete, Paris, France, pp 75–83. 1989.
[6] Manriquez, I., Diaz, S., Massone, L. Analytical and experimental cyclic response of RC walls with setback discontinuities. Proceedings of the 16th World Conference Earthquake Engineering, Santiago, Chile. 2017
[7] Massone LM, Moroder D (2009) Buckling modeling of reinforcing bars with imperfections. Eng Struct 31(3):758–767
[8] Massone LM, Orakcal K, Wallace JW. Shear–flexure interaction for structural walls. ACI Spec Publ SP–236(2):127–150. 2006.
[9] Massone, L., Rojas, F. (2012). Behavior of Reinforced Concrete Buildings (In Spanish). Mw=8.8: Earthquake in Chile, February 27 2010: 167–185. Santiago, Chile. 2012.
[10] Massone, L., F. Rojas, M. Ahumada. Analytical Study of the Response of Reinforced Concrete Walls with Discontinuities of Flag-Wall Type. Structural Concrete, 18(6): 962-973. 2017
[11] Menegotto M, Pinto PE (1973) Method of analysis of cyclically loaded reinforced concrete plane frames including changes in geometry and non-elastic behavior of elements under combined normal force and bending. In: IABSE symposium on the resistance and ultimate deformability of structures acted on by well-defined repeated loads, Lisbon
[12] Rojas. F, Anderson, J.C., and Massone, L.M. A nonlinear quadrilateral thin flat layered shell element for the modeling of reinforced concrete wall structures. Bulletin of Earthquake Engineering. 17, 6491-6513. DOI: 10.1007/s10518-019-00566-8. 2019
[13] Silva M. (2016). Analytical study of the effect of confinement and the reinforcement ratio at the boundary elements in T-shape walls. Experimental assembly design for these walls (In Spanish), Engineering Thesis, University of Chile, Chile.
[14] Thomsen, J. H., & Wallace, J. W. (1995). Displacement based design of reinforced concrete structural walls: an experimental investigation of walls with rectangular and t-shaped cross-sections, Ph.D. Thesis, Clarkson University, United States of America.
[15] Thorenfeldt E, Tomaszewicz A, Jensen JJ (1987) Mechanical properties of high-strength concrete and application in design. In: Symposium utilization of high-strength concrete, Stavanger, Norway.

